THE JOURNAL OF PHYSICAL CHEMISTRY C

Article

pubs.acs.org/JPCC

Semiconductor Nanocrystals as Luminescent Down-Shifting Layers To Enhance the Efficiency of Thin-Film CdTe/CdS and Crystalline Si Solar Cells

Sergii Kalytchuk,[†,‡] Shuchi Gupta,[†] Olga Zhovtiuk,[†] Aleksandar Vaneski,[†] Stephen V. Kershaw,[†] Huiying Fu,[§] Zhiyong Fan,[§] Eric C. H. Kwok,[∥] Chiou-Fu Wang,[∥] Wey Yang Teoh,[‡] and Andrey L. Rogach*[,†]

[†]Department of Physics and Materials Science and Centre for Functional Photonics (CFP), City University of Hong Kong, 88 Tat Chee Avenue, Kowloon, Hong Kong SAR

[‡]Clean Energy and Nanotechnology (CLEAN) Laboratory, School of Energy and Environment, City University of Hong Kong, Shatin, N.T., Hong Kong SAR

[§]Department of Electronic and Computer Engineering, Hong Kong University of Science and Technology, Clear Water Bay, Kowloon, Hong Kong SAR

[∥]Du Pont Apollo Limited, 8 Science Park West Avenue, Hong Kong Science Park, Shatin, N.T., Hong Kong SAR

Supporting Information

ABSTRACT: A simple optical model is presented to describe the influence of a planar luminescent down-shifting layer (LDSL) on the external quantum efficiencies of photovoltaic solar cells. By employing various visible light-emitting LDSLs based on CdTe quantum dots or CdSe/CdS core−shell quantum dots and tetrapods, we show enhancement in the quantum efficiencies of thin-film CdTe/CdS solar cells predominantly in the ultraviolet regime, the extent of which depends on the photoluminescence quantum yield (PLQY) of the quantum dots. Similarly, a broad enhancement in the quantum efficiencies of crystalline Si solar cells, from ultraviolet to visible regime, can be expected for an infrared emitting LDSL based on PbS quantum dots. A PLQY of 80% or higher is generally required to achieve a maximum possible short-circuit current increase of 16 and 50% for the CdTe/CdS and crystalline Si solar cells, respectively. As also demonstrated in this work, the model can be conveniently extended to incorporate LDSLs based on organic dyes or upconverting materials.

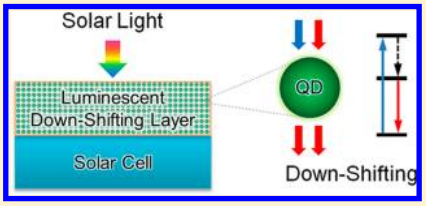

1. INTRODUCTION

Crystalline silicon and CdTe-based photovoltaics are among the leading technologies for solar power conversion, with respective laboratory-based solar cells demonstrating 25 and 18.3% efficiency and large-scale production modules reaching efficiencies of 22 and 15%.[1] One possible strategy for further efficiency improvements is to optimize the response of the photoactive materials at shorter wavelengths (blue and UV), as illustrated in Figure 1 for the CdTe-based solar cells. A commonly used thin-film CdTe/CdS solar cell is transparent to photons with energies below the bandgap energy, and an additional portion of sunlight is lost because of absorption of high-energy UV photons in the CdS buffer layer. One way to increase solar cell efficiency is to employ a luminescent down-shifting layer (LDSL), which allows for conversion of high-energy photons, which are inefficiently utilized by the photovoltaic material, to photons with energy that can be efficiently converted to electricity. In the most straightforward practice, an LDSL can be conveniently deposited on top of the existing photovoltaic material layer so that no adjustment in the overall architecture and the already optimized electrical properties is required. In recent years, several classes of

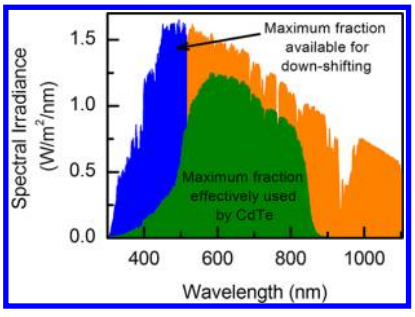

Figure 1. Global solar spectrum at air mass 1.5 showing the fraction absorbed by a typical CdTe based photovoltaic device (green) and the spectral region that can be utilized through down-shifting process (highlighted in blue).

Special Issue: Michael Grätzel Festschrift

Received: October 17, 2013
Revised: January 6, 2014

   dx.doi.org/10.1021/jp410279z | J. Phys. Chem. C XXXX, XXX, XXX−XXX

luminescent materials capable of converting a broad incident solar spectrum into photons of a narrower, longer wavelength band, such as organic dyes and lanthanide-based luminophores[2−17] and colloidal semiconductor quantum dots (QDs),[18−23] have been considered for LDSLs, alongside yet another related solar concentrator technology.[24] As compared with organic dyes and lanthanide-doped phosphors, QDs have a number of attractive optical properties: (i) an absorption that gradually increases toward shorter wavelengths (below the first absorption band) and a narrow emission band; (ii) the spectral positions of both absorption and emission are easily tunable by particle size and shape due to the quantum confinement effect; (iii) the size-dependent molar absorption coefficients at the first absorption band of QDs generally exceed those of organic dyes by one to two orders of magnitude,[25] which is combined with their superior photostability;[26] (iv) photoluminescence quantum yields (PLQYs) of properly surface-passivated QDs can reach 80−90% in the visible and near-infrared spectral ranges.[27−29]

In this work, we present a simple optical model for the analysis of the wavelength dependent efficiency of photovoltaic cells with a planar LDSL, which considers a set of the figures of merit that allow quantitative determination of the optical properties of luminescent down-conversion semiconductor nanocrystals combined with either CdTe/CdS solar cells operating in the visible spectral range or with the single crystalline Si (c-Si) solar cells with an absorption extended into the near-infrared. We show that for beneficial improvement, suitable QD-based down-conversion material with high photoluminescence quantum yield as well as proper absorption and emission profiles should be selected.

2. MATERIALS AND METHODS

2.1. c-Si and CdTe/CdS Solar Cell Devices. *CdTe/CdS Solar Cell.* The thin-film CdTe/CdS solar cells were fabricated on glass substrates coated with a transparent conducting oxide layer (TCO, fluorine-doped tin oxide) with sheet resistance of 10 ohms/square (TEC10, Pilkington). A thin CdS layer with a thickness between 60 to 150 nm was formed on the transparent conducting layer by chemical bath deposition. To improve the deposited CdS layer quality and therefore the final device efficiency, we sintered the CdS/TCO/glass substrate in a hydrogen atmosphere at a temperature between 300 and 400 °C. Thereafter, the CdTe layer was deposited onto the CdS layer by the closed space sublimation (CSS) method, with the CdS layer facing down and kept at a distance of 0.3 cm above the CdTe source. The deposition time was controlled to produce a CdTe layer with a thickness between 4 and 6 um when the CdTe source was heated to 650 to 700 °C and the glass substrate was heated to 550 to 600 °C. After deposition of the CdTe layer, saturated $CdCl_2$ solution was sprayed onto the surface of the CdTe layer, followed by annealing in a chamber with 10−20% oxygen/90−80% nitrogen atmosphere at a temperature between 380 and 430 °C. The $CdCl_2$ residue on the CdTe layer was washed away by ultrasonic cleaning in DI water. The whole substrate was dipped into $CuCl_2$ solution to introduce copper onto the CdTe layer. Subsequently, the back metal electrode, Mo/Al metal stack with a thickness of 200 nm/200 nm, was deposited onto the CdTe surface through a shadow mask, followed by annealing under nitrogen at a temperature between 150 and 250 °C for 10−30 min to reduce the contact resistance between the CdTe layer and the back electrode. Outside the back electrode area, a part of the CdTe and CdS layer was removed to expose the TCO layer, where indium was soldered to act as the front electrode. The performance parameters of such prepared solar cell are listed in Table S1 in the Supporting Information, and its external quantum efficiency as well as $J-V$ characteristics are presented in Figure S1 in the Supporting Information.

c-Si Photovoltaic Device. A c-Si solar cell pyranometer was used as purchased from Apogee Instruments, part number SP-110. The performance parameters of the latter are listed in Table S1 in the Supporting Information, and the external quantum efficiency as well as $J-V$ characteristics are presented in Figure S2 in the Supporting Information.

2.2. QD LDSL Fabrication. *QD Synthesis.* Aqueous-based CdTe QDs stabilized by thioglycolic acid were synthesized by the one-pot aqueous method of Wu et al.,[30] CdSe/CdS core/shell nanocrystals dispersed in toluene were synthesized by the successive ion layer adsorption and reaction technique of Li et al.,[31] CdSe/CdS tetrapods dispersed in toluene were synthesized according to the seeded growth approach of Talapin et al.,[32] and PbS QDs dispersed in tetrachloroethylene were synthesized following an adapted method of Moreels et al.[29] The Supporting Information provides detailed information on the synthesis details, absorption, photoluminescence spectra, and PL quantum yield values.

QD-Based Luminescent Down-Shifting Layer Deposition. Polyvinyl alcohol (PVA) and poly(methyl methacrylate) (PMMA) are known to be highly transparent polymers in the UV and in the visible spectrum (Figure S5 in the Supporting Information) and can be deposited using water and organic solvents, correspondingly. The LDSL layer was applied directly on top of the solar cell by deposition onto the surface, preliminarily cleaned with solvent, and dried. A 12% PVA solution in water was prepared by stirring at 90 °C of PVA (Mowiol 4-98, $M_w \approx 27\,000$, Aldrich) in water with further cooling to room temperature. Polymer films with two different concentrations of CdTe QDs were prepared: 5 and 20 mL of as-prepared CdTe QDs (with a molar concentration of ∼0.1 μM) were precipitated by isopropanol, centrifuged, and redissolved in 50 μL of water. The concentrated solutions obtained were carefully added to 0.5 mL of PVA solution and mechanically mixed. Films containing QDs were prepared by doctor blading using Scotch tape strips as spacers. For optical characterization, equivalent films were deposited onto glass substrates. Film thickness can be easily controlled by the number of tape strips; thin geometry is preferable to minimize parasitic optical losses (absorption and scattering by the polymer, edge emission, etc.). Slow evaporation of the water at 40 °C yielded highly transparent homogeneous luminescent films. The thickness of the QD-containing polymer film is estimated to be ∼0.1 mm.

2.3. Characterization Techniques. *Optical Measurements.* Absorption spectra were recorded using a Cary 50 UV−vis spectrophotometer (Varian) or UV-3600 UV−vis-NIR spectrophotometer (Shimadzu). Emission spectra were measured on a FLS920P fluorescence spectrometer (Edinburgh Instrument) equipped with a photomultiplier in a Peltier (air cooled) housing (R928P, Hamamatsu) or a cryogenically cooled photomultiplier (R5509-43, Hamamatsu), with a 450 W xenon arc lamp as the excitation source. The PL quantum yield, defined as the ratio between photons emitted and absorbed by the sample, was determined by an absolute method using an integrating sphere (Edinburgh Instruments) with its inner surface coated with BENFLEC, attached to the spectrofluorim-

dx.doi.org/10.1021/jp410279z | J. Phys. Chem. C XXXX, XXX, XXX−XXX

eter. Spectral correction curves for the sphere and emission detectors were provided by Edinburgh Instrument. All optical measurements were performed at room temperature under ambient conditions.

I–V Measurements. *I–V* measurements were performed using a Sun2000 11044 solar simulator (Abet, Class AAB, 1000W, continuous). Four-wire *I–V* measurements (Keithley 2400 sourcemeter) were conducted at 25 °C under a simulated AM 1.5G spectrum at one-sun intensity. The standard deviation was smaller than the quoted uncertainties of the calibration solar cell (2%) and the spatial uniformity (5%) of the solar simulator.

EQE Measurements. External quantum efficiency (EQE) measurement was performed with a monochromator, light chopper, and lock-in amplifier Protoflex QE 1400 quantum efficiency measurement system (probe beam area 2.5 mm^2, light source: halogen lamp). A calibrated silicon photodiode was used to calibrate the system with uncertainties quoted as 5% for 400–900 nm. The same photovoltaic cell was used for all layers, allowing for directly comparable results, and this also eliminated any uncertainty in spatial uniformity from the relative changes observed between different LDSLs.

2.4. Modeling of QD-Based LDSL on Top of Solar Cell: Figures of Merit. The achievable efficiency of an LDSL depends on the optical properties of the light-absorbing fluorescent material and on how well it is spectrally matched with the solar cell. The PLQY and the emission overlap (EO) integral provide figures of merit for the emission properties of individual fluorophores. The photoluminescence quantum yield, PLQY, represents the number of emitted photons N_{em} per number of absorbed photons N_{abs}: PLQY = N_{em}/N_{abs}.

Emission Overlap Integral, EO. The emission and absorption spectra of a fluorophore employed in the LDSL ideally should not overlap, which depends on the broadness of spectral peaks and the distance between their maxima (the latter quantity is termed the Stokes shift). By avoiding overlap, reabsorption is minimized within the LDSL, which otherwise would cause large efficiency drops where the QD PLQY is less than unity. Quantitatively, the emission overlap (EO), is evaluated in terms of a normalized emission profile and absorption profile of the fluorophore scaled such that 95% of the incoming light is absorbed between 300 and 400 nm (or at the maximum of a dye absorption) ($P_{em}(\lambda)$ and $P_{abs}(\lambda)$ respectively) by eq 1, as illustrated in Figure 2a. For fluorophores with no overlap between the absorption and the emission, EO would be nearly zero.

$$\mathrm{EO} = \frac{\int P_{abs}(\lambda) P_{em}(\lambda)\, d\lambda}{\int P_{em}(\lambda)\, d\lambda} \tag{1}$$

The following figures of merit are characteristics of each pair of a luminescent material and a solar cell:[33]

Emission Spectral Matching Integral (ESM). The emission spectral matching integral characterizes the overlap between the fluorophore emission and the EQE band of the solar cell. It is expressed in terms of the normalized emission profile of the fluorophore, $P_{em}(\lambda)$, and the normalized EQE of the bare solar cell, $\eta_b(\lambda)$, by eq 2 (Figure 2b). For fluorophores with emission perfectly overlapping the solar cell band, ESM would be nearly unity.

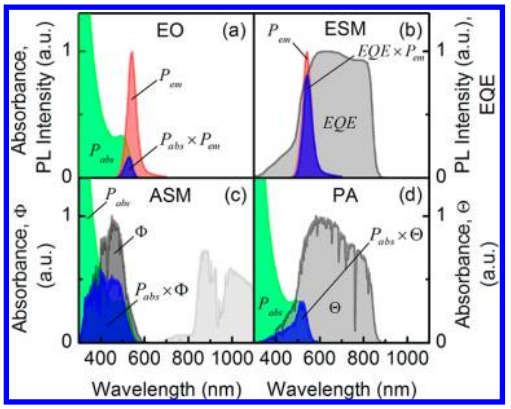

Figure 2. Schematic representation of figures of merit used in the model. (a) Emission overlap (EO) integral, (b) emission spectral matching (ESM) integral, (c) absorption spectral matching (ASM) integral, and (d) parasitic absorption (PA) integral.

$$\mathrm{ESM} = \frac{\int \eta_b(\lambda) P_{em}(\lambda)\, d\lambda}{\int P_{em}(\lambda)\, d\lambda} \tag{2}$$

Absorption Spectral Matching Integral, ASM. The absorption spectral matching integral characterizes the overlap between the fluorophore absorption and the solar spectral region that can be utilized through a down-shifting process. It is expressed in terms of the absorption profile of the fluorophore scaled such that 95% of the incoming light is absorbed between 300 and 400 nm (or at the maximum of a dye absorption), $P_{abs}(\lambda)$, and the part of the solar flux, which is not utilized by the solar cell, $\Phi(\lambda)$ (eqs 3 and 4). For fluorophores with absorption overlapping the AM1.5G fraction, which is not utilized by the solar cell, the ASM would be nearly unity.

$$\Phi(\lambda) = \mathrm{AM1.5G}(\lambda)[1 - \eta_b(\lambda)] \tag{3}$$

$$\mathrm{ASM} = \frac{\int P_{abs}(\lambda)\Phi(\lambda)\, d\lambda}{\int \Phi(\lambda)\, d\lambda} \tag{4}$$

Parasitic Absorption Integral, PA. The parasitic absorption integral characterizes the overlap between the fluorophore absorption and the solar spectral region that is effectively converted by solar cell. It is defined in terms of the absorption profile of the fluorophore scaled such that 95% of the incoming light is absorbed between 300 and 400 nm (or at the maximum of a dye absorption), $P_{em}(\lambda)$, and the part of the solar flux, which is not effectively used by the solar cell, $\Phi(\lambda)$ (eqs 5 and 6). For fluorophores with absorption not overlapping the AM 1.5G fraction, which is utilized by solar cell, PA would be nearly zero.

$$\Theta(\lambda) = \mathrm{AM1.5G}(\lambda)\eta_b(\lambda) \tag{5}$$

$$PA = \frac{\int P_{abs}(\lambda)\Theta(\lambda)\, d\lambda}{\int \Theta(\lambda)\, d\lambda} \tag{6}$$

Modeling the External Quantum Efficiency and the Short-Circuit Current Density. The efficiency of a complete solar cell including a LDSL, $\eta(\lambda)$, can be modeled using the absorption and emission spectra of the LDSL:[34]

$$\eta(\lambda) = [1 - A(\lambda)]\eta_b(\lambda) + A(\lambda)\cdot\eta_{LDSL}\cdot\max(\eta_b) \tag{7}$$

dx.doi.org/10.1021/jp410279z | J. Phys. Chem. C XXXX, XXX, XXX–XXX

where $\eta(\lambda)$ is the EQE of the LDSL-coated photovoltaic cell at a specific wavelength, $\eta_b(\lambda)$ is the EQE of the bare solar cell, $A(\lambda)$ is the fraction of solar spectrum absorbed in the LDSL, η_{LDSL} is the intrinsic LDSL efficiency, and max(η_b) is the maximum external quantum efficiency of the bare solar cell. The LDSL, η_{LDSL} (eq 8), is governed by the PLQY of the LDSL, the collection efficiency including losses due to reabsorption and light emitted away from the solar cell, CE, and the emission spectral matching integral, ESM (eq 2).

$$\eta_{LDSL} = \text{PLQY}\cdot\text{CE}\cdot\text{ESM} \tag{8}$$

For simplicity, the case of zero reabsorption of photons in the LDSL can be considered, which is a reasonable approximation for a QD-based system due to the high transparency of the LDSL in the solar cell band region.[35] In the case of isotropic emission, 50% of the light is emitted away from the photovoltaic cell. The losses due to reflection on the air−LDSL interface are calculated by the Fresnel equations and for a typical polymer or glass matrix with a refractive index ~1.5, the ideal collection efficiency is estimated to be 87%. However, the actual CE is lower due to the surface roughness and reabsorption.

The short-circuit current density, J_{sc}, is calculated by integrating the obtained EQE results with the AM 1.5G photon flux density (eq 9)[5]

$$J_{sc} = q\int_{\lambda_1}^{\lambda_2} \text{AM1.5}G(\lambda)\eta(\lambda)\,d\lambda \tag{9}$$

where q is the electron charge, AM1.5$G(\lambda)$ is the photon flux of the incident spectrum, and λ_1 and λ_2 define the range of spectrum for which the J_{sc} is to be calculated.

3. RESULTS AND DISCUSSION

3.1. Viability of Using QD-Based LDSL for Thin-Film CdTe/CdS Solar Cells. Figure 3 depicts the operation of a QD-based LDSL applied to a thin-film CdTe/CdS photovoltaic device. Incident light is utilized with high efficiency by the bare solar cell, except UV-blue light, which is absorbed by the CdS buffer layer. The CdS window layer acts as a filter that restricts the conversion of light below the bandgap (2.4 eV)[36] and is one factor that limits achievable conversion efficiencies. The QD-based LDSL is applied by depositing directly onto the bare solar cell. UV-blue light is absorbed by the QDs and re-emitted in the region of solar cell maximal efficiency. At the same time the QDs weakly absorb at longer wavelengths without affecting light in the solar cell's maximal efficiency region.

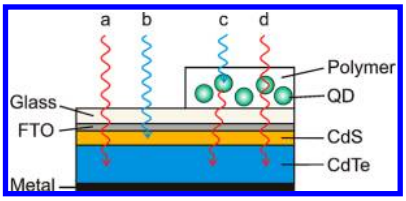

Figure 3. Schematic design of a CdTe/CdS solar cell device with a QD-based LDSL deposited on top. (a) Solar radiation is utilized in the active region of the CdTe layer (blue box), apart from high energy UV-blue light (b) which is absorbed by the CdS window layer (yellow box). (c) With the addition of the QD-based LDSL, UV-blue light is absorbed by the QDs and re-emitted in the region of preferential absorption by the solar cell. (d) QDs absorb weakly in the solar cell band's region.

Figure 4b shows the calculated efficiency of the CdTe/CdS solar cell with a CdTe QD-based LDSL based on the absorption and emission profiles of colloidal CdTe QDs (Figure 4a) for different PLQY values, assuming a collection efficiency of 87%. The increase in the EQE in the UV-blue spectral region is accompanied by a decrease in the EQE in the visible region due to parasitic absorption of the CdTe QDs in this range. The corresponding short-circuit current density variation for a range of optical densities of LDSL is presented in Figure 4c and considers the spectral range from 300 to 500 nm (lower plot) as well as a wider range from 300 to 1100 nm (upper plot). The limitation for a QD-based LDSL is clearly the emission quantum yield: relatively high PLQY values are needed to improve J_{sc}. The maximum possible increase in J_{sc}, as shown in Figure 4c, is 16% for a (realistically feasible) PLQY = 80% and an optical density of the LDSL of four absorbance units in the region of 300−400 nm.

The effect of different absorption/emission profiles (illustrated in Figure 5a) of several semiconductor nanocrystals − CdTe QDs, CdSe/CdS core/shell QDs, and CdSe/CdS tetrapods − on the calculated efficiency of a CdTe/CdS solar cell with these respective LDSLs, assuming a CE of 87% and 50% PLQY, is illustrated in Figure 5b. The LDSL employing CdSe/CdS tetrapods shows a minimal parasitic absorption and the corresponding minimal decrease of EQE in the 500−600 nm spectral range due to the optimal separation between absorption and emission profiles.

Two 2.5 nm CdTe QD-based LDSLs with different concentrations of QDs resulting in different absorption profiles (Figure 6a) were deposited on a CdTe/CdS solar cell, and the model was used to fit the measured EQE spectra (Figure 6b) using experimentally measured absorption profiles (Figure 6a, dashed lines) of LDSLs deposited onto glass substrates. Different QD concentrations directly affect the flux of the solar spectrum absorbed by the LDSL, resulting in different net yields of down-shifted photons. The concentration should be optimized because above optimal concentration will lead to high parasitic absorption in the region where the efficiency of the (bare) solar cell is initially high. Excellent agreement was obtained for simulated EQE spectra (solid lines) and the measured values (open symbols) with a fitting parameter for the collection efficiency of 14% for both CdTe QDs based LDSLs. The value of LDSL efficiency remains relatively low (14%) and is determined by a PLQY of these QDs equal to 32%. The corresponding device efficiency measured under AM 1.5G illumination with an intensity of 100 mW cm^{-2} decreased from 9.86% for bare solar cell to 9.62 and 9.08% with applied LDSL-1 and LDSL-2, respectively.

3.2. Viability of Using Near-Infrared Emitting PbS QD-Based LDSL for Crystalline Si Solar Cell. The c-Si solar cell shows significant difference in the spectral response for different parts of the solar spectrum: it works most efficiently in the 900−1100 nm spectral region and shows very low spectral response to the short-wavelength solar light (Figure 7a). While the viability of PbS NIR-emitting QDs as efficient down-shifting materials in luminescent solar concentrators has recently been addressed,[37] planar luminescent down-shifting layers based on NIR-emitting QDs have not been demonstrated yet. We have used 3.7 nm diameter PbS QDs with emission centered at 1050 nm to evaluate their viability as the LDSL applied on the c-Si cell. Figure 7b shows the calculated efficiency of c-Si photovoltaic cell with PbS a QD-based LDSL using the absorption and emission profiles of PbS QDs (Figure

dx.doi.org/10.1021/jp410279z | J. Phys. Chem. C XXXX, XXX, XXX−XXX

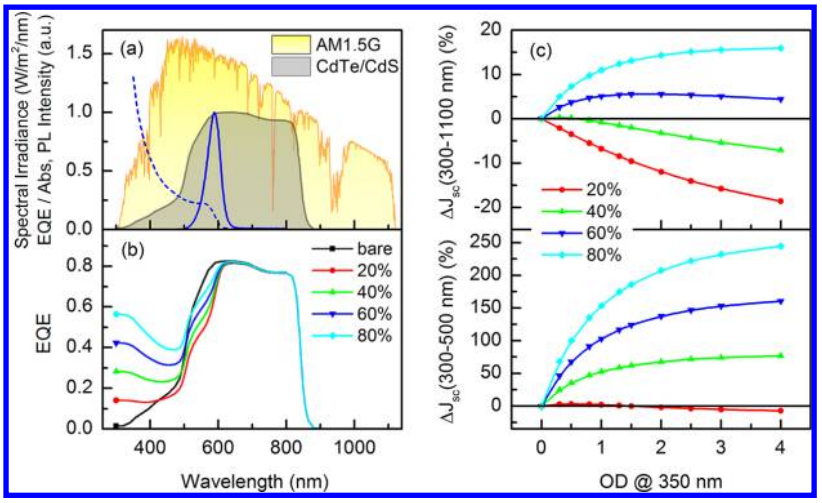

Figure 4. Calculated external quantum efficiency (EQE) and relative short-circuit current density variation spectra of a typical CdTe/CdS solar cell[5] with CdTe QD-based LDSL. (a) Absorption (dashed line) and emission (solid line) spectra of CdTe QDs in solution are shown compared with the EQE of a CdTe/CdS solar cell (highlighted in gray) and AM 1.5G spectrum (highlighted in yellow). (b) EQE spectra for different PLQY values (colored lines) compared with the bare solar cell (solid black line). (c) ΔJ_{sc} for a range of optical densities (OD) and PLQY. The lower frame takes into account the spectral range from 300 to 500 nm, while the upper frame covers the wider range from 300 to 1100 nm. For the EQE calculation purposes the absorption spectra are scaled such that 95% of the incoming light is absorbed between 300 and 400 nm. A collection efficiency of 87% was assumed.

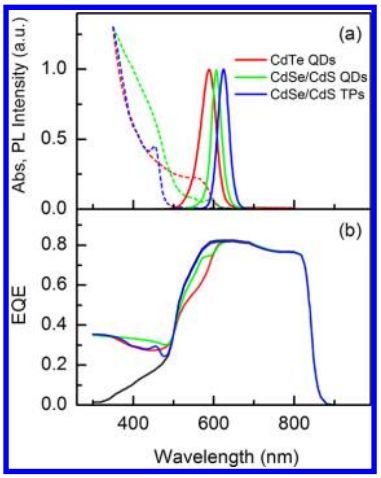

Figure 5. Calculated efficiency of a CdTe/CdS solar cell with LDSL based on different semiconductor nanocrystals. (a) Experimental absorption (dashed lines) and emission (solid lines) profiles of CdTe QDs, CdSe/CdS core/shell QDs, and CdSe/CdS tetrapods (TPs) (red, green, and blue lines, respectively). (b) Predicted performances of a solar cell with LDSL layers based on those different kinds of semiconductor nanocrystals (correspondingly colored lines), as compared with the bare CdTe/CdS solar cell (black line). The absorption spectra are set such that 95% of the incoming light is absorbed between 300 and 400 nm. A collection efficiency of 87% and PLQY of 50% were used in the calculations.

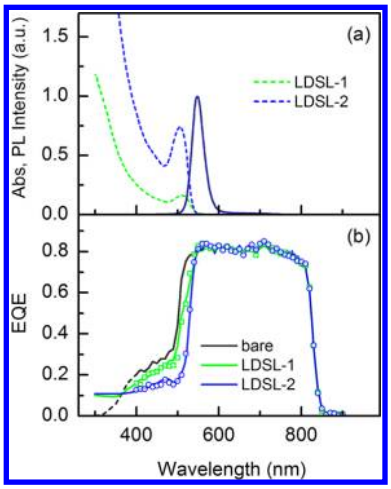

Figure 6. Experimental efficiency of a CdTe/CdS solar cell with applied CdTe QD-based LDSLs. (a) Absorption (dashed lines) and emission (solid line) spectra of CdTe QD-based LDSLs with different concentrations of QDs deposited on glass substrate (LDSL-1 and LDSL-2 as indicated). (b) Experimental (open symbols) and simulated (solid lines) external quantum efficiency spectra of the CdTe/CdS solar cell with CdTe QD-based LDSLs (green and blue line) compared with the bare CdTe/CdS solar cell (black line) showing excellent agreement between measurement and modeling.

7a) for different PLQY values, assuming a collection efficiency of 87%. The increase in the EQE in the short-wavelength region starting from a PLQY 40% is sufficient, and it grows with increasing PLQY; a slight decrease in the EQE in the 900−1100 nm range is due to parasitic absorption of the PbS QDs in this range, and it becomes less pronounced with increasing PLQY. The corresponding short-circuit current density variation for a range of optical densities of LDSL is presented in Figure 7c. The maximum possible increase in J_{sc} as shown Figure 7c is 50% for a (realistically feasible) PLQY of 80% and a LDSL optical density of 4 in the 300−400 nm range.

3.3. Figure-of-Merit Comparison. Table 1 presents figure-of-merit values for several combinations of solar cells with LDSLs: a CdTe/CdS solar cell with LDSLs based on different nanocrystals as well as on an organic dye Rhodamine 6G and PbS NIR-emitting QDs used as an LDSL of a c-Si solar cell, together with those for the commonly used NIR-emitting organic dyes. Red shaded boxes indicate critical areas of poor performance, while green shaded boxes indicate near-ideal performance. The visible-emitting organic dyes EO and ASM values are insufficient for use in practical LDSL applications. A CdTe QD-based LDSL has a larger value of the emission overlap integral due to the lower extinction coefficient

dx.doi.org/10.1021/jp410279z | J. Phys. Chem. C XXXX, XXX, XXX−XXX

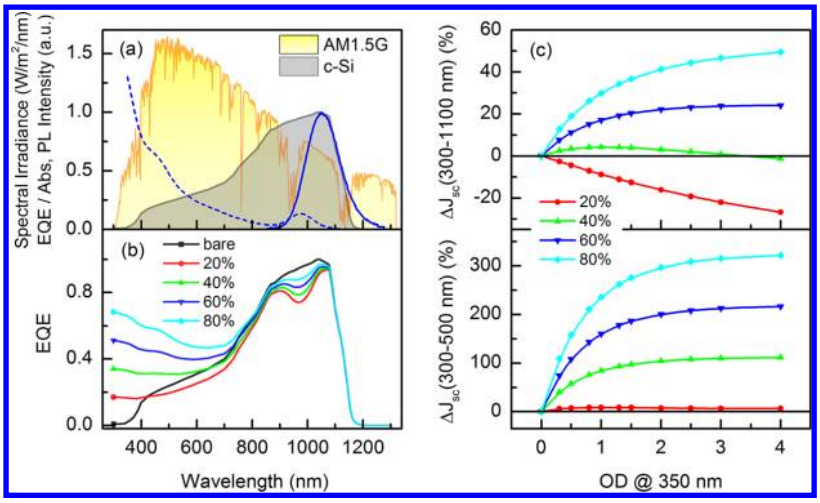

Figure 7. Calculated external quantum efficiency (EQE) and relative short-circuit current density variation spectra of a c-Si solar cell with a PbS QD-based LDSL. (a) Absorption (dashed line) and emission (solid line) spectra of PbS QDs in solution are shown compared with the relative external quantum efficiency of an Apogee c-Si solar cell pyranometer (highlighted in gray) and AM 1.5G spectrum (highlighted in yellow). (b) EQE spectra for different PLQY values (colored lines) compared with the bare solar cell (solid black line). (c) ΔJ_{sc} for a range of optical densities (OD) and PLQY. The lower frame takes into account the spectral range from 300 to 500 nm, while the upper frame covers the wider range from 300 to 1300 nm. For EQE calculation purposes, the absorption spectra are scaled such that 95% of the incoming light is absorbed between 300 and 400 nm. A collection efficiency of 87% was assumed.

Table 1. Figure-of-Merit Values for Several Combinations of LDSLs with CdTe/CdS and c-Si Solar Cells[a]

solar cell	LDSL[b]	PLQY[c], %	EO[d], %	ESM[e], %	ASM[f], %	PA[g], %
CdTe/CdS	CdTe QDs	40–80[38]	25.1	95.1	62.4	15.5
	CdSe/CdS core/shell QDs	<98[27]	8.6	99.0	70.0	11.1
	CdSe/CdS tetrapods	35–60[32]	1.4	99.8	50.6	4.6
	Rhodamine 6G	95[39]	30.9	89.6	24.5	13.4
c-Si	PbS QDs	20–90[29]	9.9	79.7	49.7	26.3
	Rhodamine 800	25[40]	16.9	55.9	23.5	14.5
	IR-26	0.05[41]	58.9	31.9	8.5	38.1
	Q Switch 5	0.05[34]	21.5	19.0	7.0	44.2

[a]Red boxes indicate critical areas of poor performance, and green boxes indicate near ideal performance. Solution phase absorption and emission spectra were used in these calculations. [b]Luminescent down-shifting layer. [c]Photoluminescence quantum yield. [d]Emission overlap. [e]Emission spectral matching. [f]Absorption spectral matching. [g]Parasitic absorption.

compared with core−shell CdSe/CdS nanocrystals. LDSLs based on CdSe/CdS tetrapods outperform the respective core−shell QDs due to the above-mentioned large global Stokes shift, leading to the reduction of the emission overlap and parasitic absorption. For the NIR-emitting LDSL, it can be seen that the PbS QD-based LDSL has superior characteristics compared with NIR organic dyes. The lower ESM value for the PbS QD-based LDSL is due to the relatively broad PL spectrum of PbS QDs, owing to their wider size distribution.

4. CONCLUSIONS

In conclusion, we have presented a simple, universally applicable optical model to analyze the wavelength-dependent efficiency of solar cells with a planar LDSL, which has been supported by experimentally obtained results on a number of semiconductor nanocrystals optically active in the visible and near-infrared. A set of figure-of-merit values allows quantitative determination of the optical properties of these luminescent materials, allowing comparison of the properties of an optimum planar LDSL combined with crystalline Si (c-Si) or thin-film CdTe/CdS solar cells. The viability of semiconductor nanocrystal down-shifting materials in planar LDSLs on CdTe/CdS and c-Si solar cells is demonstrated with a maximum possible calculated short-circuit current increase of +16 and +50% for CdTe/CdS and c-Si solar cells, respectively. The presented model can be conveniently extended to incorporate LDSL based on organic dyes or upconverting materials.

■ ASSOCIATED CONTENT

Supporting Information

Photovoltaic parameters and $J-V$ curves of CdTe/CdS and c-Si photovoltaic devices; details of the CdTe QDs, CdSe/CdS core/shell QDs and tetrapods synthesis, absorption, photoluminescence emission spectra, and PL quantum yield; transmission spectra of polymers; absorption and photo-

dx.doi.org/10.1021/jp410279z | J. Phys. Chem. C XXXX, XXX, XXX−XXX

luminescence spectra of dyes. This material is available free of charge via the Internet at http://pubs.acs.org.

AUTHOR INFORMATION

Corresponding Author

*E-mail: andrey.rogach@cityu.edu.hk. Tel: +852-3442-9532.

Notes

The authors declare no competing financial interest.

ACKNOWLEDGMENTS

This work was financially supported by the Ability R&D Energy Research Centre (AERC) of City University of Hong Kong, by grants from the Research Grant Council of the Hong Kong S.A.R., China (projects No.[T23-713/11] and 612111), and by a grant from the SRFDP/RGC Joint Research Scheme (project M_CityU102/12). H.F. and Z.F. acknowledge the technical assistance from Dr. Hungtao Chu from Clean Energy International, Inc. on CdTe device fabrication.

REFERENCES

(1) Green, M. A.; Emery, K.; Hishikawa, Y.; Warta, W.; Dunlop, E. D. Solar Cell Efficiency Tables (Version 41). *Prog. Photovoltaics* **2013**, *21*, 1−11.

(2) Klampaftis, E.; Ross, D.; McIntosh, K. R.; Richards, B. S. Enhancing the Performance of Solar Cells via Luminescent Down-Shifting of the Incident Spectrum: A Review. *Sol. Energy Mater. Sol. Cells* **2009**, *93*, 1182−1194.

(3) Richards, B. S. Enhancing the Performance of Silicon Solar Cells via the Application of Passive Luminescence Conversion Layers. *Sol. Energy Mater. Sol. Cells* **2006**, *90*, 2329−2337.

(4) Richards, B. S.; McIntosh, K. R. Overcoming the Poor Short Wavelength Spectral Response of CdS/CdTe Photovoltaic Modules via Luminescence Down-Shifting: Ray-Tracing Simulations. *Prog. Photovoltaics* **2007**, *15*, 27−34.

(5) Ross, D.; Klampaftis, E.; Fritsche, J.; Bauer, M.; Richards, B. S. Increased Short-Circuit Current Density of Production Line CdTe Mini-Module Through Luminescent Down-Shifting. *Sol. Energy Mater. Sol. Cells* **2012**, *103*, 11−16.

(6) Danos, L.; Parel, T.; Markvart, T.; Barrioz, V.; Brooks, W. S. M.; Irvine, S. J. C. Increased Efficiencies on CdTe Solar Cells via Luminescence Down-Shifting With Excitation Energy Transfer Between Dyes. *Sol. Energy Mater. Sol. Cells* **2012**, *98*, 486−490.

(7) McIntosh, K. R.; Lau, G.; Cotsell, J. N.; Hanton, K.; Derk, L.; Bettiol, F.; Richards, B. S. Increase in External Quantum Efficiency of Encapsulated Silicon Solar Cells From a Luminescent Down-Shifting Layer. *Prog. Photovoltaics* **2009**, *17*, 191−197.

(8) Klampaftis, E.; Ross, D.; Seyrling, S.; Tiwari, A. N.; Richards, B. S. Increase in Short-Wavelength Response of Encapsulated CIGS Devices By Doping the Encapsulation Layer With Luminescent Material. *Sol. Energy Mater. Sol. Cells* **2012**, *101*, 62−67.

(9) Buffa, M.; Carturan, S.; Debije, M. G.; Quaranta, A.; Maggioni, G. Dye-Doped Polysiloxane Rubbers for Luminescent Solar Concentrator Systems. *Sol. Energy Mater. Sol. Cells* **2012**, *103*, 114−118.

(10) Thomas, C. P.; Wedding, A. B.; Martin, S. O. Theoretical Enhancement of Solar Cell Efficiency By the Application of an Ideal 'Down-Shifting' Thin Film. *Sol. Energy Mater. Sol. Cells* **2012**, *98*, 455−464.

(11) Huang, X.; Han, S.; Huang, W.; Liu, X. Enhancing Solar Cell Efficiency: The Search For Luminescent Materials as Spectral Converters. *Chem. Soc. Rev.* **2013**, *42*, 173−201.

(12) van der Ende, B. M.; Aartsa, L.; Meijerink, A. Lanthanide Ions as Spectral Converters for Solar Cells. *Chem. Chem. Phys.* **2009**, *11*, 11081−11095.

(13) Donne, A. L.; Dilda, M.; Crippa, M.; Acciarri, M.; Binetti, S. Rare Earth Organic Complexes as Down-Shifters to Improve Si-Based Solar Cell Efficiency. *Opt. Mater.* **2011**, *33*, 1012−1014.

(14) Velázqueza, J. J.; Rodrígueza, V. D.; Yanes, A. C.; del-Castillo, J.; Méndez-Ramos, J. Down-Shifting in Ce^{3+}-Tb^{3+} Co-Doped SiO_2-LaF_3 Nano-Glass-Ceramics for Photon Conversion in Solar Cells. *Opt. Mater.* **2012**, *34*, 1994−1997.

(15) Yang, G.; Zhou, S.; Lin, H.; Teng, H. Down-Conversion Near Infrared Emission in Pr^{3+}, Yb^{3+} Co-Doped Y_2O_3 Transparent Ceramics. *Physica B* **2011**, *406*, 3588−3591.

(16) Fix, T.; Rinnert, H.; Blamire, M. G.; Slaoui, A.; MacManus-Driscoll, J. L. Nd:$SrTiO_3$ Thin Films as Photon Downshifting Layers for Photovoltaics. *Sol. Energy Mater. Sol. Cells* **2012**, *102*, 71−74.

(17) Shalav, A.; Richards, B. S.; Green, M. A. Luminescent Layers for Enhanced Silicon Solar Cell Performance: Up-Conversion. *Sol. Energy Mater. Sol. Cells* **2007**, *91*, 829−842.

(18) Muffler, H.-J.; Bar, M.; Lauermann, I.; Rahne, K.; Schroder, M.; Lux-Steiner, M. C.; Fischer, C.-H.; Niesen, T. P.; Karg, F. Colloid Attachment by ILGAR-Layers: Creating Fluorescing Layers to Increase Quantum Efficiency of Solar Cells. *Sol. Energy Mater. Sol. Cells* **2006**, *90*, 3143−3150.

(19) Cheng, Z.; Su, F.; Pan, L.; Cao, M.; Sun, Z. CdS Quantum Dot-Embedded Silica Film as Luminescent Down-Shifting Layer for Crystalline Si Solar Cells. *J. Alloys Compd.* **2010**, *494*, L7−L10.

(20) Rothemunda, R.; Kreuzera, S.; Umunduma, T.; Meinhardtb, G.; Fromherza, T.; Jantscha, W. External Quantum Efficiency Analysis of Si Solar Cells with II-VI Nanocrystal Luminescent Down-Shifting Layers. *Energy Procedia* **2011**, *10*, 83−87.

(21) Pi, X.; Li, Q.; Li, D.; Yang, D. Spin-Coating Silicon-Quantum-Dot Ink to Improve Solar Cell Efficiency. *Sol. Energy Mater. Sol. Cells* **2011**, *95*, 2941−2945.

(22) Chen, H.-C.; Lin, C.-C.; Han, H.-V.; Chen, K.-J.; Tsai, Y.-L.; Chang, Y.-A.; Shih, M.-H.; Kuo, H.-C.; Yu, P. Enhancement of Power Conversion Efficiency in GaAs Solar Cells with Dual-Layer Quantum Dots Using Flexible PDMS Film. *Sol. Energy Mater. Sol. Cells* **2012**, *104*, 92−96.

(23) Hodgsonn, S. D.; Brooks, W. S. M.; Clayton, A. J.; Kartopu, G.; Barrioz, V.; Irvine, S. J. C. Enhancing Blue Photoresponse in CdTe Photovoltaics by Luminescent Down-Shifting Using Semiconductor Quantum Dot/PMMA Films. *Nano Energy* **2013**, *2*, 21−27.

(24) Purcell-Milton, F.; Gun'ko, Y. K. Quantum Dots for Luminescent Solar Concentrators. *J. Mater. Chem.* **2012**, *22*, 16687−16697.

(25) Resch-Genger, U.; Grabolle, M.; Cavaliere-Jaricot, S.; Nitschke, R.; Nann, T. Quantum Dots Versus Organic Dyes as Fluorescent Labels. *Nat. Methods* **2008**, *5*, 763−775.

(26) Wu, X.; Liu, H.; Liu, J.; Haley, K. N.; Treadway, J. A.; Larson, J. P.; Ge, N.; Peale, F.; Bruchez, M. P. Immunofluorescent Labeling of Cancer Marker Her2 and Other Cellular Targets with Semiconductor Quantum Dots. *Nat. Biotechnol.* **2002**, *21*, 41−46.

(27) Greytak, A. B.; Allen, P. M.; Liu, W.; Zhao, J.; Young, E. R.; Popovic, Z.; Walker, B. J.; Nocera, D. G.; Bawendi, M. G. Alternating Layer Addition Approach to CdSe/CdS Core/Shell Quantum Dots With Near-Unity Quantum Yield and High On-Time Fractions. *Chem. Sci.* **2012**, *3*, 2028−2034.

(28) Chen, O.; Zhao, J.; Chauhan, V. P.; Cui, J.; Wong, C.; Harris, D. K.; Wei, H.; Han, H.-S.; Fukumura, D.; Jain, R. K.; et al. Compact High-Quality CdSe-CdS Core-Shell Nanocrystals with Narrow Emission Linewidths and Suppressed Blinking. *Nat. Mater.* **2013**, *12*, 445−451.

(29) Moreels, I.; Justo, Y.; Geyter, B. D.; Haustraete, K.; Martins, J. C.; Hens, Z. Size-Tunable, Bright, and Stable PbS Quantum Dots: A Surface Chemistry Study. *ACS Nano* **2011**, *5*, 2004−2012.

(30) Wu, S.; Dou, J.; Zhang, J.; Zhang, S. A Simple and Economical One-Pot Method to Synthesize High-Quality Water Soluble CdTe QDs. *J. Mater. Chem.* **2012**, *22*, 14573−14578.

(31) Li, J. J.; Wang, Y. A.; Guo, W.; Keay, J. C.; Mishima, T. D.; Johnson, M. B.; Peng, X. Large-Scale Synthesis of Nearly Monodisperse CdSe/CdS Core/Shell Nanocrystals Using Air-Stable Reagents Via Successive Ion Layer Adsorption and Reaction. *J. Am. Chem. Soc.* **2003**, *125*, 12567−12575.

(32) Talapin, D. V.; Nelson, J. H.; Shevchenko, E. V.; Aloni, S.; Sadtler, B.; Alivisatos, A. P. Seeded Growth of Highly Luminescent CdSe/CdS Nanoheterostructures with Rod and Tetrapod Morphologies. *Nano Lett.* **2007**, *7*, 2951−2959.
(33) Alonso-Alvarez, D.; Ross, D.; Richard, B. S. Luminescent Down-Shifting for CdTe Solar Cells: A Review of Dyes and Simulation of Performance. *IEEE Photovoltaic Spec. Conf., 38th* **2012**, 9−14.
(34) Geyer, S. M.; Scherer, J. M.; Moloto, N.; Jaworski, F. B.; Bawendi, M. G. Efficient Luminescent Down-Shifting Detectors Based on Colloidal Quantum Dots for Dual-Band Detection Applications. *ACS Nano* **2011**, *5*, 5566−5571.
(35) Wilson, L. R.; Rowan, B. C.; Robertson, N.; Moudam, O.; Jones, A. C.; Richards, B. S. Characterization and Reduction of Reabsorption Losses in Luminescent Solar Concentrators. *Appl. Opt.* **2010**, *49*, 1651−1661.
(36) Luque, A.; Hegedus, S. *Handbook of Photovoltaic Science and Engineering*; John Wiley & Sons, Ltd.: Chichester, U.K., 2003.
(37) Shcherbatyuk, G. V.; Inman, R. H.; Wang, C.; Winston, R.; Ghosh, S. Viability of Using Near Infrared PbS Quantum Dots as Active Materials in Luminescent Solar Concentrators. *Appl. Phys. Lett.* **2010**, *96*, 191901−191903.
(38) Rogach, A. L.; Franzl, T.; Klar, T. A.; Feldmann, J.; Gaponik, N.; Lesnyak, V.; Shavel, A.; Eychmüller, A.; Rakovich, Y. P.; Donegan, J. F. Aqueous Synthesis of Thiol-Capped CdTe Nanocrystals: State-of-the-Art. *J. Phys. Chem. C* **2007**, *111*, 14628−14637.
(39) Kubin, R. F.; Fletcher, A. N. Fluorescence Quantum Yields of Some Rhodamine Dyes. *J. Lumin.* **1982**, *27*, 455−462.
(40) Alessi, A.; Salvalaggio, M.; Ruzzon, G. Rhodamine 800 as Reference Substance for Fluorescence Quantum Yield Measurements in Deep Red Emission Range. *J. Lumin.* **2013**, *134*, 385−389.
(41) Semonin, O. E.; Johnson, J. C.; Luther, J. M.; Midgett, A. G.; Nozik, A. J.; Beard, M. C. Absolute Photoluminescence Quantum Yields of IR-26 Dye, PbS, and PbSe Quantum Dots. *J. Phys. Chem. Lett.* **2010**, *1*, 2445−2450.